geosciences

MDPI

Article

Time-Dependent Proppant Pack Conductivity and Hydraulic Fracture Design

Danil Kashapov, Mikhail Turbakov *, Alsu Ivanova, Evgenii Kozhevnikov, Evgenii Riabokon, Zakhar Ivanov and Dmitrii Kobiakov

Department of Oil and Gas Technologies, Perm National Research Polytechnic University, Perm 614990, Russia; dokashapov@pstu.ru (D.K.); zgivanov@pstu.ru (A.I.); kev@pstu.ru (E.K.); riabokon@pstu.ru (E.R.); zakharivanov@pstu.ru (Z.I.); dvkobjakov@pstu.ru (D.K.)
* Correspondence: msturbakov@pstu.ru

Abstract

Proppant selection requires an understanding of whether greater crush resistance translates into better flow performance under sustained loading. Short-term crush tests were compared with conductivity and permeability measurements over 60 h at 54.3 MPa and 86 °C for nominal 16/20 and 20/40 mesh fractions of a polymer-coated magnesia–quartz ceramic proppant. At 68.95 MPa, the crushed fraction was 8.88% for 16/20 and 2.27% for 20/40. After 60 h, the packs retained 81.4% and 77.7% of their initial conductivity, respectively, and 77.9% and 80.7% of their initial permeability. The greater crush resistance and permeability retention of the 20/40 fraction therefore did not extend to conductivity retention. Because conductivity also depends on pack thickness, permeability retention alone does not determine conductivity retention. Treating initial conductivity as a constant overestimates its value at 60 h by 22.9% for 16/20 and 28.7% for 20/40. A separate model recalculation using recorded treatment data illustrates how operating conditions affect predicted fracture geometry and spatially averaged conductivity.

Keywords: ceramic proppant; conductivity loss; retained permeability; hydraulic fracturing; fracture design

1. Introduction

In low-permeability and geologically complex reservoirs, hydraulic fracturing must create a conductive fracture system that maintains a flow path to the wellbore after treatment. Fracture initiation, propagation, and proppant placement involve coupled rock deformation and fluid flow. Laboratory and numerical analyses of fracture initiation and propagation depend on the imposed stress regime, specimen geometry, fluid properties, and representation of fracture mechanics [1]. Fracture taper and operating conditions also affect proppant transport and placement [2]. Experiments on shale-like cores from different depths of the same well show that rock-fabric heterogeneity affects breakdown pressure, fracture-growth rate, and fracture opening [3]. Once placed, the proppant supports the fracture walls and provides the pore space for production flow. Particle-size distribution, grain shape, and crush resistance are therefore routinely considered in material selection [4]. Fracture design also requires the flow properties of the proppant pack under sustained loading at reservoir temperature and in contact with fluid [5].

Classical fracture models link aperture and propagation to fluid pressure, elasticity and fluid loss. Perkins and Kern developed fracture-width estimates [6], Nordgren treated

Check for updates

Academic Editor: Huaibo Song

Received: 25 September 2026
Revised: 27 October 2026
Accepted: 4 November 2026
Published: 6 November 2026

Copyright: © 2026 by the authors. Licensee MDPI, Basel, Switzerland. This article is an open access article distributed under the terms and conditions of the Creative Commons Attribution (CC BY) license.

propagation with limited vertical extent and fluid loss [7], and Geertsma and de Klerk provided rapid estimates of fracture width and extent [8].

As a fracture closes, grain crushing produces fines and alters the pore structure of the proppant pack. Zheng et al. [9] used post-crush particle-size distributions to estimate the permeability of packs containing Jordan and Genoa quartz sands, resin-coated sand and ceramic proppant. The highest predicted permeabilities at 40 MPa were obtained for 20/40 and 30/50 ceramic proppants and 20/40 resin-coated sand. Grain embedment into the fracture walls [10,11], rearrangement and local compaction [12,13] also change fracture flow properties. Rock–fluid interaction can reduce conductivity through rock spalling and particle migration [14] or swelling of clay minerals [15].

Propped fracture conductivity also depends on loading duration. Pearson et al. [16,17] conducted extended conductivity tests on sand and lightweight ceramic proppants. In tests lasting up to 250 days, conductivity continued to decline beyond the 50 h reference measurement. Conductivity retention must therefore be defined for a specified loading period and reference state.

Conductivity loss affects production forecasts. Pearson and Fowler [18] evaluated its long-term effect on recovery for different fracture parameters. Kim et al. [19] incorporated pressure-dependent fracture closure into a gas-production model. Over 392 days, the predicted aperture decreased by 8.5% and the effective permeability of the block within the stimulated region by 54.2%. Including closure reduced the mismatch in cumulative production from 5.5% to less than 1% when matching the same well history.

Selecting a size fraction requires relating short-term crushing to the flow properties retained after a specified period under load. Permeability estimates based on post-crush particle-size distributions [9] and extended conductivity tests [16,17] describe different responses. Neither establishes whether a fraction that generates fewer fines will retain more of both its permeability and its conductivity. For a coated magnesia–quartz proppant, this relationship can be examined by comparing crushing and both normalized flow properties for the same nominal size fractions.

We test the hypothesis that the fraction with a lower crushed mass fraction retains more of its initial permeability and conductivity under sustained loading. Short-term crush tests on nominal 16/20 and 20/40 mesh polymer-coated magnesia–quartz ceramic proppants are compared with 60 h flow tests at 86 °C and 54.3 MPa. The comparison establishes whether the ranking by crush resistance also applies to permeability and conductivity retention, quantifies the differences between these selection criteria and evaluates their consequences for time-dependent flow parameters.

2. Materials and Methods

2.1. Material and Measurements

The tested material was a polymer-coated magnesia–quartz ceramic proppant in nominal 16/20 and 20/40 mesh fractions. This class of proppant is manufactured from magnesium silicates and quartz sand (SiO_2) [20]. The designation refers to the material class; the phase composition and coating properties of the tested batch were not determined.

Bulk density, acid solubility, particle-size distribution and grain crushing were assessed using two determinations per condition. Conductivity and permeability were analyzed from one time series for each nominal size fraction. Sample standard deviations from duplicate determinations describe repeatability; no confidence interval or statistical significance is assigned to the individual flow histories.

2.2. Physical Properties and Crush Testing

Physical properties were measured using procedures based on GOST R 51761-2013 [4]. Bulk density was determined from the mass of material in a measuring vessel with a nominal volume of 100 cm^3. It includes intergranular voids in the loosely packed material and differs from the apparent particle density required for settling calculations.

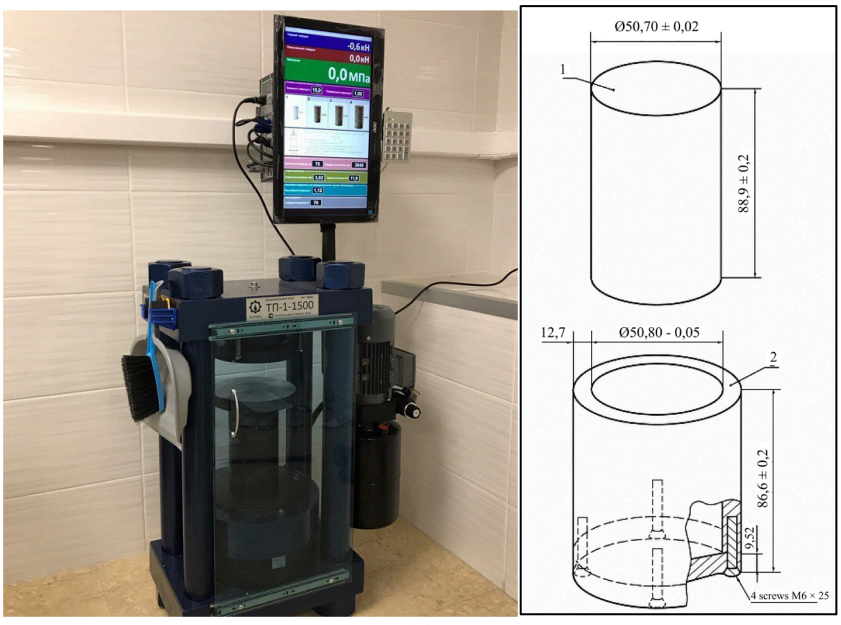
Acid solubility was determined from the mass lost in a mixture of hydrochloric acid and ammonium bifluoride. The mixture was prepared from 46 g of NH_4HF_2 and 361 mL of 37 wt% HCl, cooled and diluted to 1 L. Approximately 5 g of dried proppant was immersed in 100 mL of the solution at 66 °C for 30 min. The residue was filtered, dried at 105 °C to constant mass and weighed. This test measures resistance to the specified acid mixture.

Sieve analysis was performed with a SWING 200 sieve shaker (MEZOS, Hradec Králové, Czech Republic) using a nominal sample mass of 100 g, a sieving time of 10 min and a balance with a stated resolution of 0.01 g. The mass retained on each sieve was divided by the initial sample mass. The original 20/40 mesh records contain inconsistent sieve designations, which were retained because the actual sieve sizes could not be established. Grain shape was assessed visually using the Krumbein–Sloss chart.

Short-term crush tests were conducted in a crush cell loaded with a TP-1-1500 hydraulic test press (Testpress LLC, Misailovo, Moscow Region, Russia) (Figure 1a). The target stress was reached over 1 min and held for 2 min.

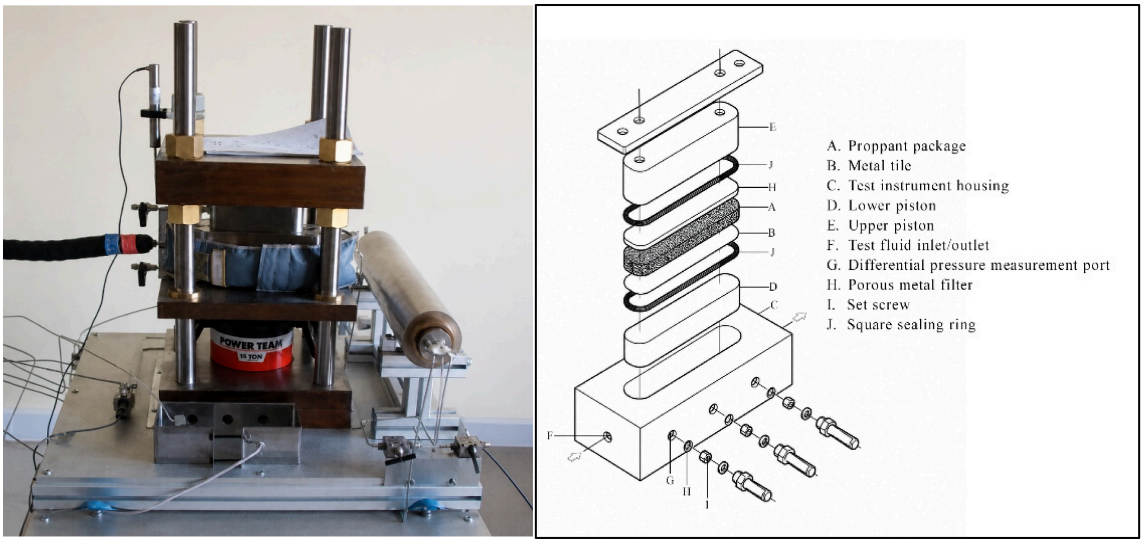
After unloading, the material was sieved for 10 min. The mass of fines generated was expressed as a percentage of the initial sample mass. Applied stresses were 5000, 7500 and 10,000 psi (34.47, 51.71 and 68.95 MPa). These conditions differed from those of the 60 h flow tests.

For the crush tests, points show the means of two determinations and error bars span the minimum and maximum values. The three means for each size fraction were fitted separately by least squares after logarithmic transformation, $\ln f = \ln a + b\sigma$. Solid lines show the exponential fits over 34.47–68.95 MPa, and dotted lines extend them to 30 and 69 MPa, where comparison data are available. Sensitivity to the choice of function was assessed using an alternative two-parameter power-law fit. Neither fit used the literature data. The logarithmic ordinate shows the crushed fraction as *a* mass percentage.



(**a**)

Figure 1. *Cont.*



(**b**)

Figure 1. Laboratory equipment: (**a**) TP-1-1500 hydraulic test press and proppant crush cell; (**b**) modified conductivity cell. In the crush-cell drawing, 1 denotes the piston and 2 the cell body; dimensions are in millimeters.

2.3. Conductivity Testing and Data Analysis

Conductivity was measured over time in a modified linear-flow cell (Figure 1b) using a procedure based on ISO 13503-5:2006 [5]. The test description specifies 2 wt% KCl solution, a nominal flow rate of 5 mL/min, a temperature of 86 °C and a final normal stress of 7870 psi (54.3 MPa). The loading steps were 1000, 2000, 4000, 6000 and 7870 psi (6.89, 13.79, 27.58, 41.37 and 54.26 MPa). Time in the analyzed series begins at the final stress level, with measurements at 0, 15, 30, 45 and 60 h.

Flow properties were analyzed as ratios within each time series. The reported viscosity of 1.02 mPa·s has not been verified at 86 °C, and the stated areal proppant loading of 39 kg/m^2 is inconsistent with the pack thickness inferred from paired conductivity and permeability values. These uncertainties affect absolute conductivity. For any constant rescaling of viscosity, calculated conductivity and permeability change by the same proportional amount, while their within-series retention ratios remain unchanged. This cancelation requires viscosity to remain constant in time within each test.

For Darcy flow through a pack with a rectangular cross-section, conductivity is related to the measured quantities by

$$C_f = k_f w = \left(\frac{Q\mu L}{A\Delta P}\right) w = \frac{Q\mu L}{W\Delta P} \quad (1)$$

Here, conductivity denotes proppant-pack flow capacity (permeability multiplied by loaded pack thickness), not hydraulic conductivity in units of velocity. Permeability denotes single-phase pack permeability in the KCl tests; no relative-permeability function is evaluated. In Equation (1), C_f is pack conductivity, k_f is permeability, w is pack thickness under load, Q is volumetric flow rate, μ is viscosity, L is the distance between pressure taps, A is the flow cross-sectional area, W is cell width and ΔP is the pressure drop, with $A = Ww$. A constant multiplicative error in μ, L, W or another factor cancels when each value is divided by the initial value. Normalization does not remove time-varying errors in flow rate, temperature, viscosity, pressure or geometry.

Conductivity retention was calculated as $R(t) = 100 \cdot C_f(t)/C_f(0)$, and normalized permeability as $k_f(t)/k_f(0)$. Since $C_f = k_f\, w$, the two ratios can differ when pack thickness changes. Applying conductivity retention again to the same local conductivity as a perme-

ability correction would count the change twice. The decline over the final interval was calculated relative to the value at 45 h. The overestimate arising from a constant initial parameter was calculated as the initial-to-final ratio minus one.

For comparison with published data, time was expressed in hours and conductivity in mD·m, with 1 mD·ft = 0.3048 mD·m and 1 μm^2·cm = 10.1325 mD·m. The values at 1 and 2 h from Wang J. et al. [21] were digitized from the published conductivity plots using linear calibration; the error bars represent a reading uncertainty of ±2 pixels. Both fractions were tested at 50 MPa and 5 kg/m^2 in distilled water; temperature was not specified for these plots. For the 40/70 ceramic proppant, Liu et al. [22] reported the fitted relation $C_f(t) = 10.1325[1.512\exp(-60t/417.465) + 2.090]$, evaluated over 0–50 h at 50 MPa, 60 °C and 5 kg/m^2. Time begins at the start of this hold, following loading steps of 5, 20 and 35 MPa.

Yan et al. [23] reported the conductivity of 20/40 ceramic proppant after 60 h at 40 MPa and 10 kg/m^2, using formation water and rock plates with an elastic modulus of 7284 MPa; the temperature was not specified. In these comparisons, the lines joining points aid comparison, whereas the dashed Liu curve represents the published fit. Curves are confined to the time intervals reported in each source. The legends identify the source and size fraction. Color distinguishes the fractions tested here; circles, squares and diamonds denote 16/20, 20/40 and 30/50, respectively. An open inverted triangle marks an upper bound. Curves derived solely from fits have no measurement markers.

2.4. Reservoir and Fracturing Treatment

A hydraulic fracturing treatment in a Lower Cretaceous sandstone–siltstone reservoir provides a field example. The treated interval contains clay interbeds. Well logs indicate a porosity of 15–25% and a permeability of approximately 0.66 mD; the reported temperature and reservoir pressure are 86 °C and 54.4 MPa.

A diagnostic minifrac preceded the main treatment. The original summary gives instantaneous shut-in pressures of 34.35 MPa at the wellhead and 69.10 MPa at the bottomhole. Closure was identified 123 min after shut-in, at 29.59 and 64.43 MPa, respectively. The approximately 34.8 MPa difference between the surface and bottomhole pressures represents the hydrostatic head after pumping stops, rather than frictional loss during flow. Bottomhole closure pressure reflects the total stress acting on the fracture. Subtracting the initial reservoir pressure gives approximately 10.0 MPa, provided that fracture-fluid pressure has equilibrated with reservoir pressure. The laboratory normal stress of 54.3 MPa is a separate test boundary condition and is not equated with the in situ closure stress. An independently verified target depth and stress gradient are not available for this field example.

The treatment used 724 m^3 of fluid, including 11 m^3 of $CaCl_2$-based brine, and 200 t of proppant: 195 t of 20/40 mesh and 5 t of 16/20 mesh. The treatment description specifies a viscoelastic carrier fluid, a gradual increase in proppant concentration and a final proppant-free displacement stage.

2.5. Model Comparison and Permeability Retention

The design model was compared with a recalculation using the recorded pumping schedule and pressure history. Inputs included time-dependent injection rate, proppant concentration and pressure, fluid rheology, leakoff data from the diagnostic minifrac and depth-dependent geomechanical properties. The pumping records are field measurements; fracture height, aperture, length and conductivity are model outputs. The numerical depth profiles and a calibration history are not documented in the source record. No stress-dependent matrix-permeability or porosity function, or dependence on proppant roundness, is specified for this comparison.

For each parameter, the relative change was calculated as the recalculated value minus the design value, divided by the design value and multiplied by 100. It measures the model response to incorporating the treatment data.

A maximum hydraulic fracture half-length of 300 m was imposed as a model constraint.

Conductivity was averaged over the propped area using element areas as weights:

$$C_f = \frac{\sum_{i=1}^{N} C_{f,i} A_i}{\sum_{i=1}^{N} A_i} \quad (2)$$

where $C_{f,i}$ is local conductivity, A_i is element area and N is the number of propped elements. A permeability retention factor was additionally applied to the productive intervals:

$$C_{f,eff} = R_p \cdot \frac{\sum_{j=1}^{m} C_{f,j} h_j}{\sum_{j=1}^{m} h_j} \quad (3)$$

where $C_{f,eff}$ is effective conductivity, R_p is the dimensionless permeability retention factor, $C_{f,j}$ is the local conductivity of productive interval j, h_j is its thickness and m is the number of productive intervals. Equations (2) and (3) average over different regions, so the resulting conductivities are not interchangeable. *Rp* is a phenomenological multiplier, not a separately measured property of the tested material. Its numerical value and time dependence are unspecified in the original calculation, so its individual contribution is not inferred from the paired model outputs.

A design calculation requires a defined test duration, reference state and treatment of permeability retention. If R_p is the ratio of retained to initial permeability for a single pack under unchanged conditions, $R_p(t) = k_f(t)/k_f(0)$ directly defines its time dependence. When $C_{f,j}(t)$ is calculated from $k_f(t)$ and $w(t)$, multiplying it by $R_p(t)$ again would double-count the same permeability change. The relation $R_p(t) = k_f(t)/k_f(0)$ applies only when that change has not already been included in local conductivity and pack thickness is specified consistently.

3. Results

3.1. Physical Properties and Grain Crushing

The mean bulk densities of both nominal fractions round to 1.41 g/cm^3 at the recorded precision (Table 1). The recalculated mean acid solubilities were 5.95% and 4.73%, respectively (Table 1). Both values are below the 8% threshold cited for comparison in the original test description; this comparison does not establish compliance of the polymer-coated magnesia–quartz ceramic proppant with the cited standard.

Table 1. Duplicate determinations of bulk density and acid solubility, with means and sample standard deviations (SD; n = 2). A zero displayed SD indicates identical recorded readings, not zero measurement uncertainty.

Parameter	Fraction	Determination 1	Determination 2	Mean ± SD
Bulk density, g/cm^3	16/20	1.41	1.41	1.41 ± 0.00
Bulk density, g/cm^3	20/40	1.40	1.41	1.41 ± 0.01
Acid solubility, %	16/20	5.96	5.93	5.95 ± 0.02
Acid solubility, %	20/40	4.78	4.67	4.73 ± 0.08

For the 16/20 mesh fraction, the combined retained masses on the No. 18 and No. 20 sieves were 94.18% and 94.61%, giving a recalculated mean of 94.40% (Figure 2). For the 20/40 mesh fraction, the sieve sequence in the graph is consistent with the source summary table, whereas the detailed test results assign the same retained masses to differently

designated sieves. The reported mass fraction within the nominal size range of 97.61% cannot therefore be verified. The 20/40 designation is retained as the nominal sample label without confirming that the particle-size distribution corresponds to this fraction. The comparison therefore concerns the two labeled samples and does not isolate particle size as a causal variable. Both fractions had a reported sphericity of 0.9 and roundness of 0.8.

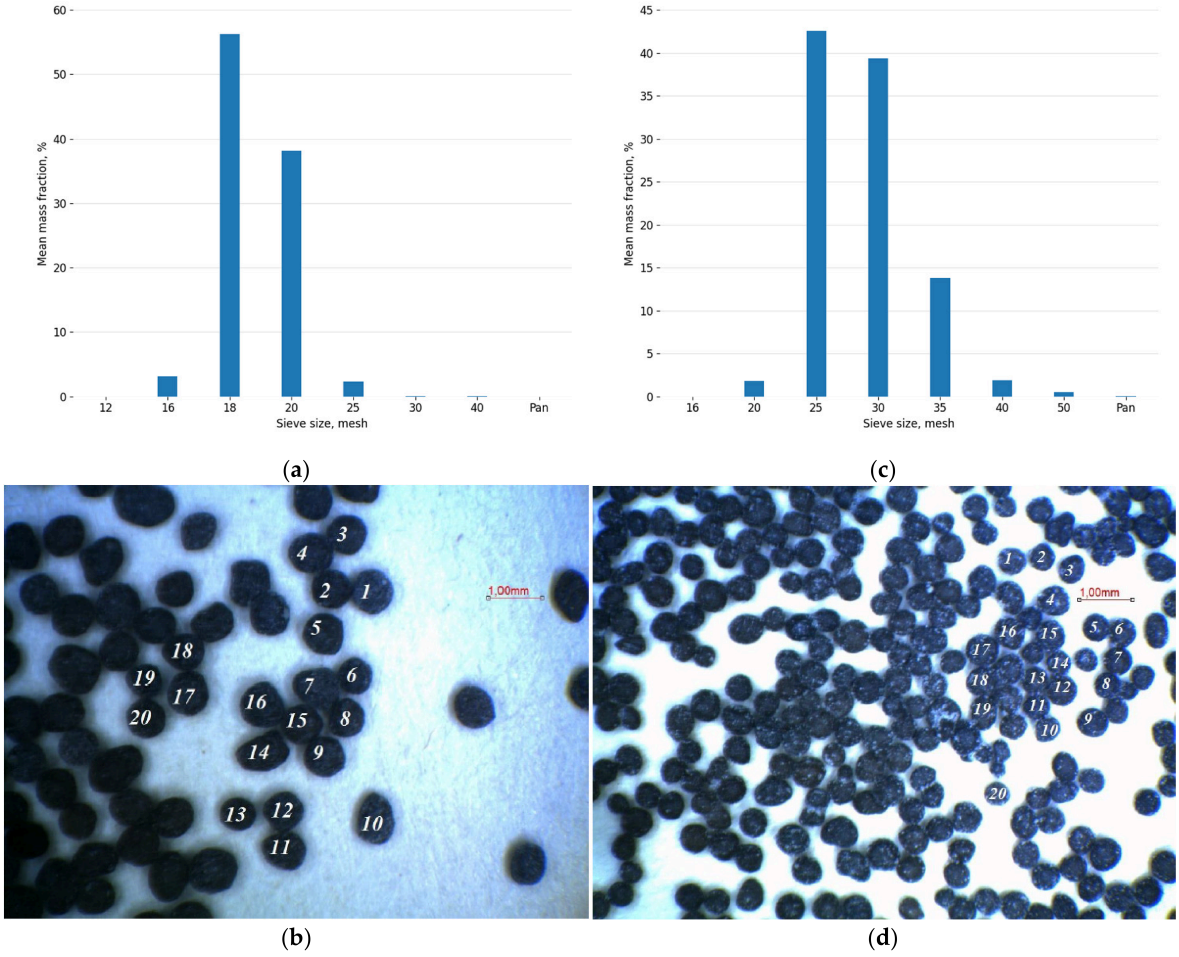


Figure 2. Mean pretest retained masses on sieves and particle images for the nominal 16/20 (**a**,**b**) and 20/40 (**c**,**d**) fractions. Numbers in the particle images identify individual grains. The short-term crush tests quantify total generated fines; a complete post-loading size distribution is not available.

The mass fraction of crushed grains increased with closure stress for both fractions (Figure 3). At 10,000 psi, duplicate determinations for the 16/20 fraction gave 9.23% and 8.52%, with a mean of 8.88%; the corresponding values for the 20/40 fraction were 2.21% and 2.32%, with a mean of 2.27%. The sample standard deviations at this stress were 0.50 and 0.08 percentage points, respectively ($n = 2$). In the short-term tests, the nominal 20/40 sample generated fewer fines.

Figure 3 includes the literature data for the 20/40 ceramic proppant: Anaya et al. [24], 7.8 ± 0.1% at 34.5 MPa (source-reported standard deviation; API 19C); Xu et al. [25], 1.4% at 52 MPa for untreated material (loading for 1 min and a 2 min hold); and Ren et al. [26], 20.22% at 69 MPa for material without soaking (2 min hold). Wang W. et al. [27] reported <0.5% for the uncoated 30/50 ceramic proppant and 0.1% for the coated material at 30 MPa after 2 min; the marker for the uncoated material denotes an upper bound. Material compositions and sieve-analysis criteria differ, and loading details are not reported in all sources.

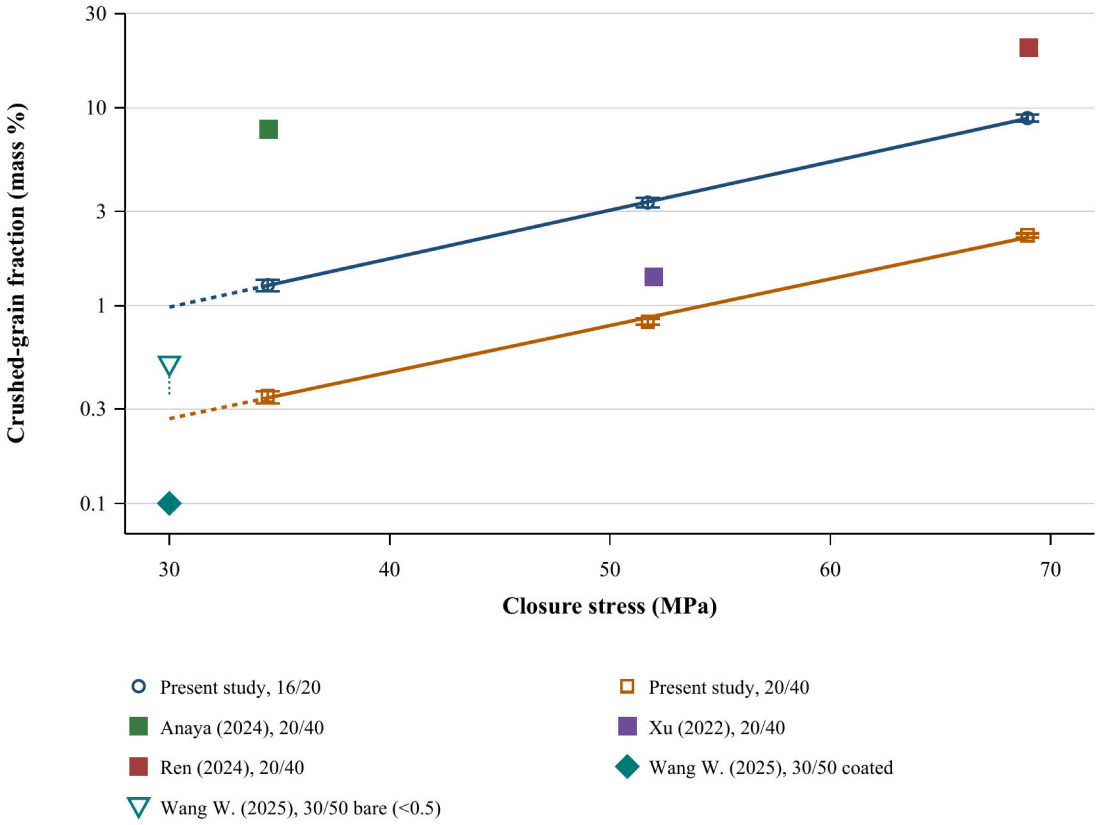


Figure 3. Mass fraction of crushed grains as a function of closure stress: present 16/20 (open circles) and 20/40 (open squares) samples, fitted curves, and published ceramic-proppant data from Anaya et al. [24] (square at 34.5 MPa), Xu et al. [25] (square at 52 MPa), Ren et al. [26] (square at 69 MPa), and Wang W. et al. [27] (diamond: coated 30/50; inverted triangle: uncoated 30/50 upper bound). Present-study points are duplicate means; error bars span the minimum and maximum determinations.

The mean values were fitted by $f = 0.181043 \exp(0.0564033\sigma)$ for 16/20 and $f = 0.0527257 \exp(0.0542228\sigma)$ for 20/40, where f is the mass fraction in percent and σ is stress in MPa. The root-mean-square deviations from the fitted curves were 0.025 and 0.039 percentage points, respectively. Extrapolation to 30 MPa gives 0.983% and 0.268% from the exponential relations, whereas alternative two-parameter power-law relations give 0.823% and 0.227%. These ranges characterize sensitivity to the model form and are not confidence intervals. The 0.1% value for polymer-coated ceramic proppant reported by Wang W. et al. is below both extrapolations [27]. The published 20/40 values vary in their agreement with the fitted curve in Figure 3 [24–26]; the combined data do not follow a single crushing relation. At the final flow-test stress of 54.26 MPa, the present exponential fits interpolate crushed fractions of 3.86% and 1.00% for 16/20 and 20/40, respectively. This preserves the fitted crushing order at that stress but does not reproduce the loading history or duration of the flow tests.

Wang W. et al. showed that a coating can retain fragments and reduce the fines content measured by sieving without establishing that the grains themselves remain intact [27]. Zheng et al. compared Jordan and Genoa quartz sands, resin-coated sand, and the ceramic proppant. Based on the characteristics of particles after crushing, the highest calculated permeability at 40 MPa was obtained for 20/40 and 30/50 ceramic proppants and 20/40 resin-coated sand [9]. Wei et al. reported that crushing of quartz sand from one source was approximately 20–40% lower than that of sand from another source at 35 MPa [28]. Material composition, grain size, and test conditions must be considered when relating crushing results to conductivity.

3.2. Changes During the 60 h Conductivity Tests

After 60 h, conductivity retention was 81.4% for the 16/20 fraction and 77.7% for the 20/40 fraction; the corresponding normalized permeabilities were 77.9% and 80.7% (Figure 4). The ranking of the fractions differs between these two metrics.

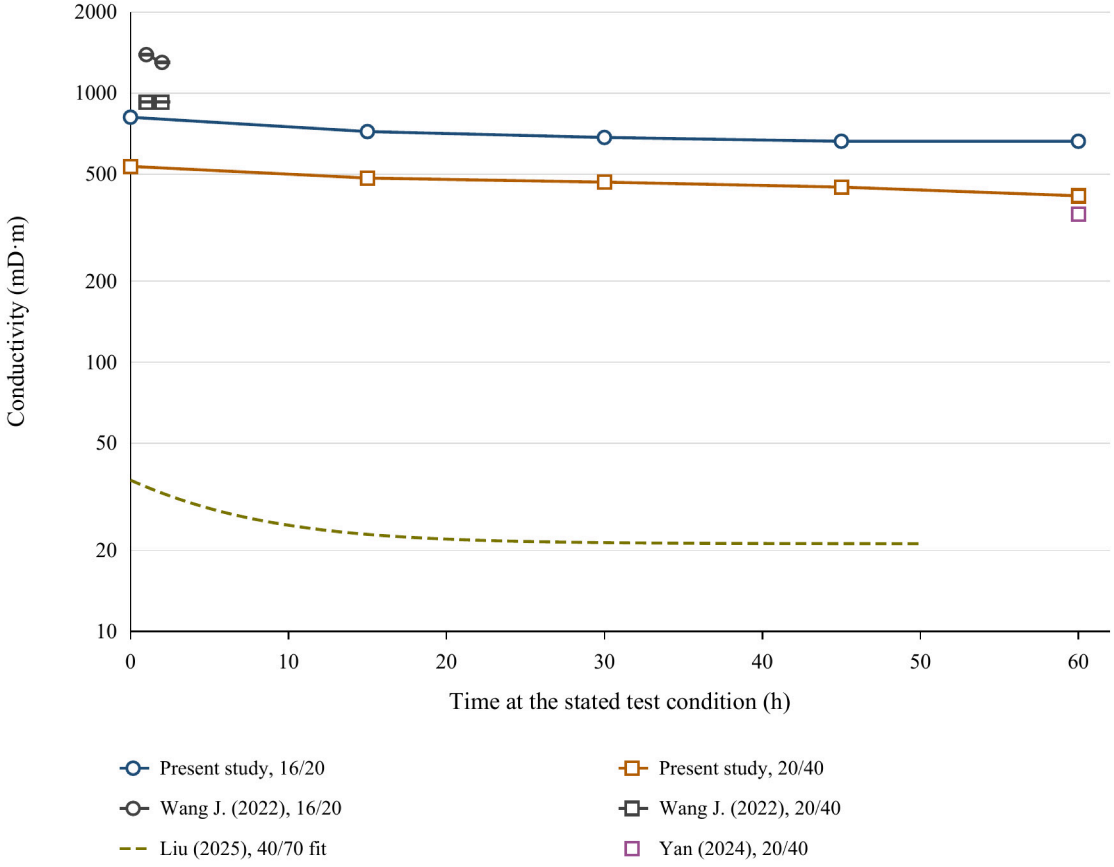


Figure 4. Conductivity change with time in this study and published studies. The present 16/20 and 20/40 series lose 18.6% and 22.3% of their respective initial conductivity after 60 h, retaining 81.4% and 77.7%. Literature data are from Wang J. et al. [21] (16/20: circles; 20/40: squares), Liu et al. [22] (40/70: dashed fitted curve), and Yan et al. [23] (20/40: isolated square at 60 h). The data retain their source-specific reference states and reported time intervals.

For the 16/20 fraction, conductivity values at 45 and 60 h were identical to the stated precision, consistent with a plateau over the final 15 h interval. For the 20/40 fraction, conductivity decreased from 447.8 to 415.4 mD·m over the same interval, a further 7.2% relative to the value at the start of that interval.

Absolute conductivity values in Figure 4 differ substantially even after conversion to common units. The Liu et al. fit gives 58.1% retention of initial conductivity after 50 h [22]. Yan et al. report 23.3% after 60 h relative to an initial value whose exact measurement time is not specified [23]; only the final point with a confirmed time is shown in the figure. Particle size, areal proppant loading, temperature, fluid, rock plates, and loading history differ across the studies, so the data do not define a common rate of conductivity loss.

3.3. Design Calculation and Post-Treatment Model Recalculation

In the reported post-treatment model recalculation, fracture height at the wellbore decreased from 100 to 93 m (−7.0%), mean aperture from 5.44 to 4.45 mm (−18.2%), and maximum propped half-length increased from 195 to 213 m (+9.2%). The area-weighted

conductivity changed from 55.18 to 56.74 mD·m (+2.8%), while effective conductivity changed from 50.39 to 62.27 mD·m (+23.6%).

The increase in effective conductivity substantially exceeds that in area-weighted conductivity. Equations (2) and (3) define these quantities over different averaging domains. Effective conductivity also depends on the permeability retention factor and the weights of productive intervals.

Using the recorded pumping and pressure data changed both the modeled aperture distribution (Figure 5) and the overall fracture geometry and conductivity (Figure 6).

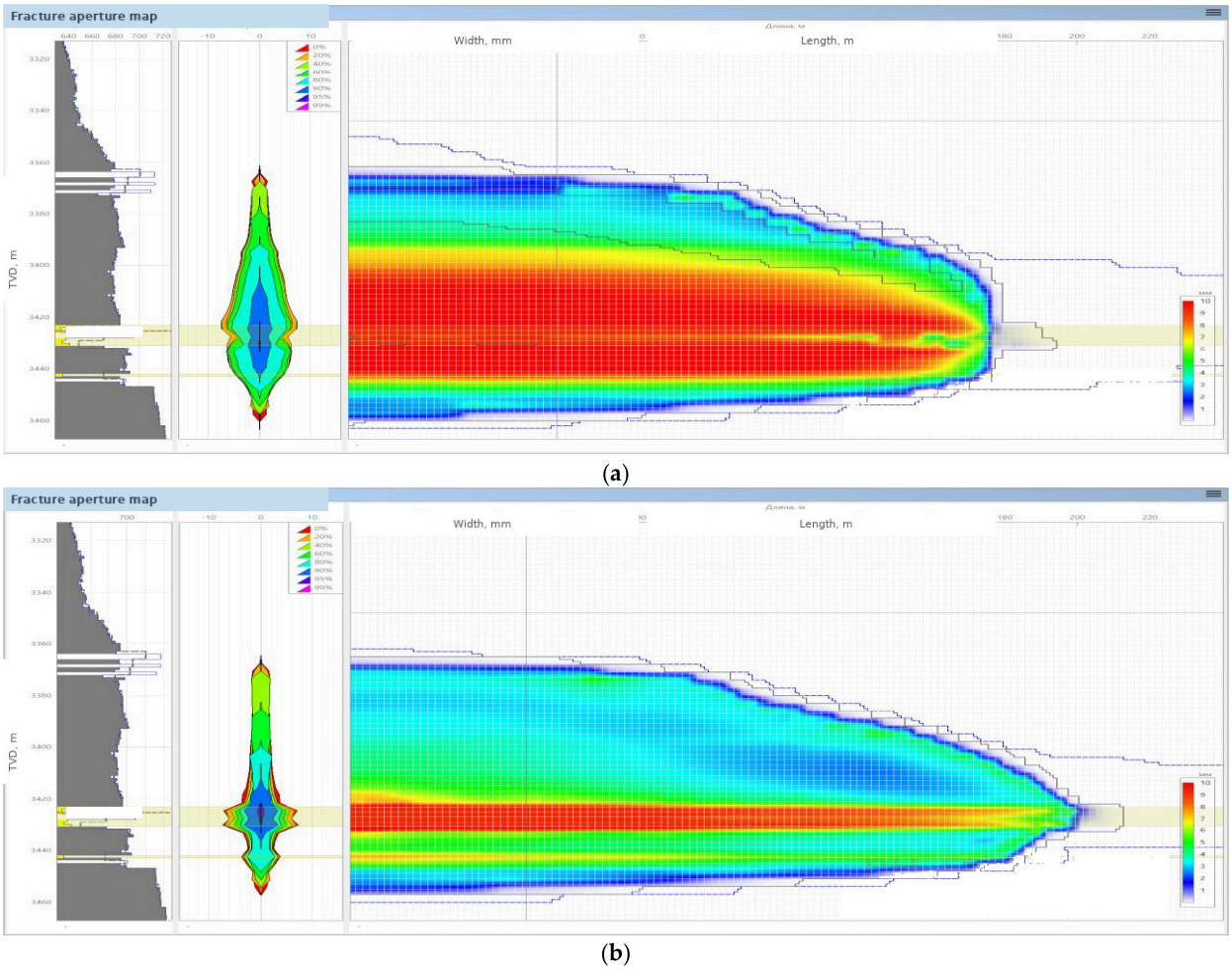


Figure 5. Modeled fracture-aperture maps for the design calculation (**a**) and recalculation with recorded treatment data (**b**). The color scale at the right of each map gives aperture in millimeters. Both maps describe the same treatment with 195 t of nominal 20/40 and 5 t of nominal 16/20 proppant.

3.4. Effect of Using Initial Flow Properties

If the constant initial value $C_f(0)$ is used instead of $C_f(60\,\mathrm{h})$, the relative overestimation, $C_f(0)/C_f(60\ \mathrm{h}) - 1$, is 22.9% for the 16/20 mesh fraction and 28.7% for the 20/40 mesh fraction. For permeability, $k_f(0)/k_f(60\ \mathrm{h}) - 1$ is 28.4% and 23.9%, respectively. Normalized conductivity and permeability may differ when pack thickness changes: $C_f(t)/C_f(0) = [k_f(t)/k_f(0)][w(t)/w(0)]$. Therefore, normalized conductivity cannot substitute for $R_p(t)$ without accounting for the change in pack thickness.

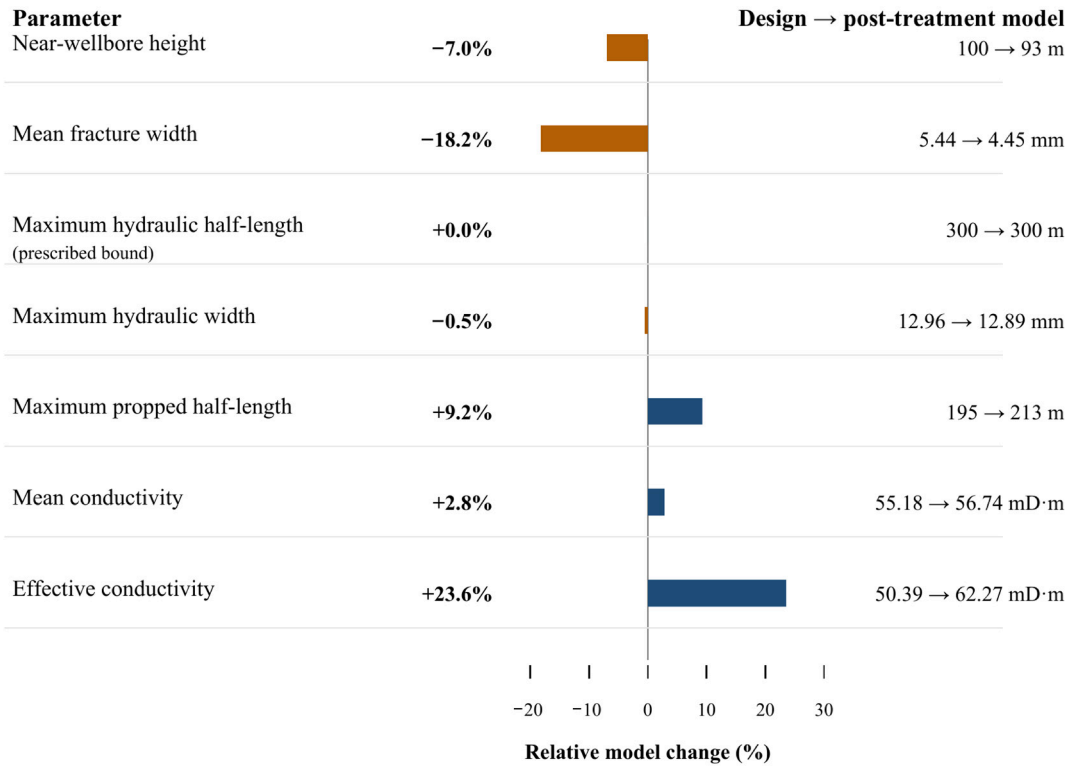


Figure 6. Relative changes and paired model outputs obtained by replacing design inputs with the recorded treatment inputs.

4. Discussion

4.1. Comparison with Published Proppant Tests and Fracture Models

Grain crush resistance and conductivity retention of the proppant pack characterize different aspects of proppant performance. At 68.95 MPa, the 20/40 fraction generated fewer fines than the 16/20 fraction; however, its conductivity retention after 60 h at 54.3 MPa was lower (Table 2).

Table 2. Crushed fraction, proppant embedment, and flow responses under the reported laboratory and modeling conditions. Conductivity retention is the ratio of the final to the initial value; where indicated, values were calculated from fitted relations. Conductivity units: 1 μm^2·cm = 10.1325 mD·m; 1 D·cm = 10 mD·m.

Study and Conditions	Result	Basis for Comparison
Present study Crushing: 68.95 MPa, 2 min. Flow: 54.3 MPa, 86 °C, 60 h; 2 wt% KCl.	For 16/20 and 20/40, respectively: crushed fractions of 8.88% and 2.27%; conductivity retention of 81.4% and 77.7%; normalized permeability of 77.9% and 80.7%.	Two nominal fractions; means of two crush determinations and one flow-property time series per fraction.
Zheng et al. [9] Jordan and Genoa quartz sands, resin-coated sand, and ceramic proppant; three fractions, loaded to 40 MPa.	At 40 MPa, the highest calculated permeability values in the investigated series were obtained for 20/40 and 30/50 ceramic proppant and 20/40 resin-coated sand.	Permeability was estimated from post-crush particle characteristics.

Table 2. *Cont.*

Study and Conditions	Result	Basis for Comparison
Anaya et al. [24] 20/40 ceramic proppant; API 19C crush tests at 34.5 MPa.	Crushed fractions of 7.8–17.2 wt% for eight combinations of composition and firing schedule; 7.8 ± 0.1 wt% for the formulation containing 20 wt% glass after firing at 1100 °C.	Composition and firing schedule varied at a common size fraction and test stress; the spread is the standard deviation reported by the source.
Ren et al. [26] 20/40 fraction; steel plates; formation water. Flow at 35, 42, 52, and 69 MPa for 50 h per step; 7.5–10 kg/m^2.	Unsoaked ceramic proppant: 20.22% fines after a separate 2 min test at 69 MPa and 32.21% after 200 h of flow; composite proppant: 20.62% and 32.84%, respectively. Post-flow values for soaked samples were 37.97% and 40.63%.	Post-flow sieving was compared with short crush-cell tests. Loading history and fluid exposure differed.
Bandara et al. [11] Siltstone contact during water injection; five loading cycles to 17.5 MPa.	Proppant embedment depths: 1.10 mm for sand, 0.63 mm for ceramic proppant, and 0.29 mm for polymer-coated proppant.	Material effect on proppant embedment in rock under cyclic loading.
Zhang et al. [14] Barnett Shale fractures; water flow; closure stress of 27.6 MPa.	Conductivity decreased by up to 88% after water flow.	Conductivity change in propped shale fractures during water flow.
Sun et al. [29] Initial pack thickness of 5 mm; 5 mL/min; stress steps from 10 to 70 MPa for 25 min each.	At 70 MPa, conductivity was 62 μm^2·cm for 20/40 ceramic proppant and 3 μm^2·cm for 20/40 quartz sand. A 3:1 sand–ceramic mixture by volume had conductivity 1.27–3 times that of pure sand over the investigated stress range.	The areal proppant loadings of pure ceramic proppant and sand were 7.3 and 7.7 kg/m^2. Mixture masses were selected for an initial pack thickness of 5 mm.
Zhang et al. [30] Conglomerate plates; 8 kg/m^2; 2% KCl; 50 h hold at each stress step.	As stress increased from 27.6 to 69 MPa, the conductivity of 20/40 quartz sand decreased from 27.9 to 0.4 D·cm; at 69 MPa, the conductivity of 40/70 ceramic proppant was 3.5 D·cm.	Conductivity after sequential loading holds; stress and cumulative test duration varied simultaneously.
Yan et al. [23] 30/50 ceramic proppant; 55 MPa; 60 h; 10 kg/m^2; rock elastic modulus of 3696 MPa.	Formation water: a decrease from 75.19 to 16.09 μm^2·cm, with 21.4% of the initial conductivity retained. Fracturing fluid: from 109.49 to 11.03 μm^2·cm, with 10.1% retained.	Conductivity retention was calculated from the reported initial and final values for each fluid; test temperature was not reported.
Liu et al. [22] 50 MPa stress step; 60 °C; 50 h; shale plates; 2 mL/min.	Conductivity retention determined from fits: 40/70 ceramic proppant, 5 kg/m^2, 58.1%; 70/140 ceramic proppant, 5 kg/m^2, 53.7%; 40/70 quartz sand, 5 kg/m^2, 51.8%; 40/70 ceramic proppant, 2.5 kg/m^2, 52.6%.	Ratios of calculated values at 3000 and 0 min of the final step in the 5–20–35–50 MPa sequence.
Wu et al. [31] 30/50:40/70 ceramic proppant, 3:1 by mass; 105 MPa; 150 °C; 72 h; 10 wt% KCl.	Sequential placement and uniform mixing: conductivity retention of 66% and 57% at 7.5 kg/m^2, and 40% and 28% at 5 kg/m^2, respectively.	Conductivity retention was calculated by subtracting reported losses from 100%. Under sequential placement, fine grains were placed at the inlet and coarse grains at the outlet.
Kim et al. [19] Model matched to production history; 0–392 days.	Calculated fracture aperture decreased from 1.000 to 0.915 mm; effective block permeability decreased from 3.2808 to 1.5010 mD.	Calculated fracture aperture and effective block permeability in the stimulated near-wellbore region.

Short crush-cell tests and extended flow tests sample different damage states, as illustrated by the experiments of Ren et al. [26]. For unsoaked 20/40 ceramic proppant, the fines fraction was 20.22% after 2 min at 69 MPa and 32.21% after 200 h of flow with four consecutive 50 h loading steps ending at 69 MPa. The corresponding values for the composite proppant were 20.62% and 32.84%. The approximately 12-percentage-point increase reflects the combined effects of loading history and fluid exposure.

At 50 MPa and 60 °C, fitted curves reported by Liu et al. [22] give 50 h conductivity retention of 58.1% for the 40/70 ceramic proppant at an areal proppant loading of 5 kg/m^2, 53.7% for 70/140 ceramic proppant at the same loading, 51.8% for 40/70 quartz sand, and 52.6% for 40/70 ceramic proppant at 2.5 kg/m^2. Both particle size and areal proppant loading affected retained flow capacity. In the present tests at 54.3 MPa and 86 °C, the two nominal fractions retained 77.7–81.4% conductivity after 60 h.

At a closure stress close to that used here, Yan et al. [23] measured fluid-dependent conductivity losses in packs bounded by rock. For the 30/50 ceramic proppant at 55 MPa, 10 kg/m^2, and 60 h, conductivity decreased from 75.19 to 16.09 μm^2·cm in the formation water and from 109.49 to 11.03 μm^2·cm in fracturing fluid. The corresponding retentions were 21.4% and 10.1%, compared with 77.7–81.4% in the present 2 wt% KCl tests.

Bandara et al. [10] found that placement of mixed grain sizes reduced aperture loss and the increase in fracture tortuosity relative to the single-size proppant. Walsh et al. [12] observed local proppant-pack failure and large-scale grain rearrangement with increasing confining pressure. Voltolini and Ajo-Franklin [13] identified grain rearrangement, breakage, and fracture–wall interaction by microtomography and flow calculations. These processes can alter both pore connectivity and fracture aperture.

Conductivity decline can continue beyond the initial loading period. Pearson et al. [16] tested four sand or lightweight ceramic proppants for up to 250 days at 51.7 MPa and recorded further conductivity decline after the 50 h reference measurement. In a subsequent study, three 40/70 materials were tested for 1000 h at 121.1 °C and 2.44 kg/m^2 [17]. In the present study, the conductivity of the 16/20 fraction did not change during the final 15 h. Mittal et al. [32] also examined permeability and compaction under simulated reservoir conditions, including grain breakage, fines migration, grain embedment into the rock, and diagenetic changes.

Liu et al. [22] incorporated a fitted laboratory conductivity-decline relation into a production model and compared calculated cumulative gas production with a well history. Their model cases varied proppant type, size, and areal proppant loading. Ren et al. [26] supplemented laboratory material tests with a field study comprising one test well and two control wells.

Field comparisons also indicate that the required conductivity depends on in situ stress. Zhang et al. [30] reported mean oil rates of 20.1 t/d for 14 wells treated with sand and 19.6 t/d for 17 wells treated with ceramic proppant at depths shallower than 3300 m. At depths greater than 3500 m, the mean rate was 27.1 t/d for 16 wells treated with a 50:50 sand–ceramic mixture and 36.9 t/d for 27 wells treated with the ceramic proppant. These were treatment cohorts for which proppant and fluid volumes also differed. The greater separation at depth accompanied higher closure stresses and lower sand-pack conductivity measured in the same study.

Pearson and Fowler [18] used extended-time conductivity-decline data in recovery calculations for different completion designs. Kim et al. [19] incorporated fracture closure into production-history matching: simulated fracture aperture decreased by 8.5%, and effective permeability of the stimulated-region block decreased by 54.2% over 392 days (Table 2). After closure was included, the cumulative-production matching error decreased from 5.5% to below 1%; this quantifies agreement with the production history used for

model calibration. The reported $R^2 = 0.9855$ refers to the fitted permeability–pressure relation. In the present study, incorporating operational data increased area-weighted conductivity by 2.8% and effective conductivity by 23.6%. These changes characterize the calculated distribution and averaging of conductivity, whereas the error reported by Kim et al. [19] characterizes agreement with production history.

At the proppant-pack scale, Xu et al. compared a conductivity model with cell measurements [33], and Bolintineanu et al. compared simulated geometry with X-ray microtomography data [34]. Sang et al. reported final conductivity equal to 37.8% of the initial value for a ceramic-propped fracture between flat plates at 50 MPa and 25 °C [35]. Those tests were conducted separately from experiments on unpropped fractures that retained aperture.

4.2. Grain Size and Retention of Flow Properties

The 20/40 fraction generated fewer fines in the short-term crush tests and retained 2.8 percentage points more of its initial permeability after 60 h than 16/20, but its conductivity retention was 3.7 percentage points lower. The hypothesized common ranking by crush resistance and retention of both flow properties was not observed for these two individual histories; the differences are descriptive and do not establish a population ranking. This comparison concerns relative changes over 60 h rather than absolute conductivity. Zheng et al. [9] related post-crush particle characteristics to estimated permeability; the time series obtained here distinguish permeability retention from conductivity retention for the same fractions. Fragment retention by the coating [27], pack rearrangement and wall contact may contribute to the difference, although their individual contributions require direct observation.

Conductivity retention exceeds normalized permeability by 3.5 percentage points for 16/20 and is 3.0 percentage points lower for 20/40. From $C_f = k_f w$, equal relative changes in conductivity and permeability imply constant pack thickness. Dividing normalized conductivity by normalized permeability gives an algebraically inferred thickness ratio of 1.045 for 16/20 and 0.963 for 20/40 at 60 h. These ratios are not measurements of deformation and require independent loaded-width measurements for verification. Using initial conductivity throughout the 60 h period overestimates the endpoint value by 22.9% for 16/20 and 28.7% for 20/40.

A retention factor in a flow calculation must describe the property being updated. If local conductivity has already been calculated from the changing permeability, applying R_p again would double-count that change. Permeability, conductivity and pack thickness must be specified consistently. In the field example, recalculation with the actual pumping schedule and pressure response also changed the spatial conductivity distribution; area-weighted and effective conductivity average this distribution over different regions.

Mixture composition affects conductivity at a given grain size. At 70 MPa and an initial pack thickness of 5 mm, Sun et al. [29] measured conductivities of 62 μm²·cm for the 20/40 ceramic proppant and 3 μm²·cm for quartz sand. Adding 25 vol% ceramic proppant to 20/40 sand increased conductivity by a factor of 1.27–3 relative to pure sand over the investigated stress range. After flow testing, the crushed fraction was 21.22–45.68% for the 20/40 mixtures and 12.30–30.39% for the 40/70 mixtures. Mixtures of smaller fractions generated fewer fines, whereas packs of coarser grains had higher conductivity.

Wu et al. [31] evaluated placement effects for a 3:1 mass mixture of 30/50 and 40/70 ceramic proppant at 105 MPa and 150 °C. At 7.5 kg/m², sequential placement retained 66% conductivity after 72 h, compared with 57% for uniform mixing; at 5 kg/m², the respective values were 40% and 28%. Sequential placement provided an advantage of 9–12 percentage points at fixed material composition.

Acid mass loss characterizes resistance to a specified acid mixture, whereas bulk density describes a loose granular packing with interparticle voids [4]. Anaya et al. [24] reported bulk densities of 1.26–1.38 g/cm^3 for different ceramic formulations, close to the present mean bulk densities, both reported as 1.41 g/cm^3 at the recorded precision. Their crushed fractions nevertheless ranged from 7.8% to 17.2% at 34.5 MPa. Similar bulk density does not imply identical grain-crushing resistance.

Fluid composition also affects flow through the adjacent rock. Cheng and Milsch [36] observed a permeability decrease of approximately 1.5 orders of magnitude in illite-bearing sandstone during heating to 145 °C and a further decrease of comparable magnitude when a previously introduced 2 M NaCl solution was diluted to below 0.5 M. Confining and pore pressures were 10 and 1 MPa, respectively. In water-saturated, unpropped Fontainebleau sandstone fractures at 1 MPa pore pressure, hydraulic aperture decreased from 57 to 54 µm as confining pressure increased from 5 to 30 MPa at room temperature, and from 58 to 41 µm during heating to 140 °C at 10 MPa confining pressure [37].

4.3. Applicability of Laboratory and Modeling Results

The retention factors characterize two 60 h proppant-pack time series under the specified laboratory conditions. Normalization cancels a constant scale factor, whereas time-dependent errors in fluid properties, flow rate, and pressure measurement remain. Independent replicate flow tests and records of pack thickness are unavailable. The 3.7-percentage-point difference in conductivity retention is an observed contrast between two packs. A differential time-dependent scaling of more than approximately 4.8% between the two endpoint-to-initial ratios could reverse this ordering; a constant scale error within either series would not. Determining absolute downhole conductivity requires verified fluid properties, areal proppant loading, and loaded pack thickness.

Physical properties and grain breakage were evaluated in two determinations for each condition on the tested samples. The sieve identifiers for 20/40 remain unresolved; this label is therefore used as a nominal sample designation. Each breakage relation was fitted to three mean values at different stresses, and its extrapolation depends on the model form. Only coated material was tested; the observed ranking is not extrapolated to the uncoated proppant, quartz sand, other coatings, or independently verified size classes. Coating characterization, post-flow particle-size analysis, and direct observation of proppant-pack deformation were outside the experimental program. The comparison describes the combined material response under the test conditions.

The original design calculation and the post-treatment model recalculation used different operational inputs. Their differences characterize the model update; assessment of predictive accuracy requires paired calculations and independent observations of fracture geometry or production. The reported fracture height at the wellbore of 93 m differs from the 92 m interval inferred from the source depth marks, whose reference datum also conflicts with Figure 5. The aperture profiles are therefore interpreted as model outputs rather than independent measurements of fracture position or height containment.

5. Conclusions

For the two tested nominal samples of polymer-coated magnesia–quartz ceramic proppant, the short-term crushing and 60 h conductivity-retention rankings differed. At 68.95 MPa, the crushed fraction was 2.27% for 20/40 and 8.88% for 16/20. After 60 h at 54.3 MPa and 86 °C, the 20/40 fraction retained less of its initial conductivity, 77.7% versus 81.4%, but more of its initial permeability, 80.7% versus 77.9%. Lower fines generation alone did not identify the fraction with better retention of both flow properties.

Time-dependent conductivity and permeability must be assigned consistently with pack thickness. Using initial conductivity as a constant overestimated its 60 h value by 22.9% for 16/20 and 28.7% for 20/40 under the tested conditions. In the separate field example, recalculation with pumping and pressure data increased area-weighted conductivity by 2.8% and effective conductivity by 23.6%, reflecting changes in the predicted conductivity distribution and its spatial averaging.

Author Contributions: Conceptualization, M.T. and E.R.; methodology, E.K.; software, D.K. (Danil Kashapov); validation, D.K. (Danil Kashapov), D.K. (Dmitrii Kobiakov), A.I. and Z.I.; formal analysis, E.R.; investigation, D.K. (Danil Kashapov); resources, M.T.; data curation, D.K. (Danil Kashapov); writing—original draft preparation, A.I.; writing—review and editing, D.K. (Dmitrii Kobiakov); visualization, Z.I. and A.I.; supervision, M.T.; project administration, E.K.; funding acquisition, M.T. All authors have read and agreed to the published version of the manuscript.

Funding: The research was funded by the Ministry of Science and Higher Education of the Russian Federation (Project No. FSNM-2026-0005).

Data Availability Statement: The numerical values reported in this article are available in the text, tables, and figures. Original instrument logs and individual conductivity-test records are unavailable.

Acknowledgments: ChatGPT-6.1 (OpenAI) assisted with the translation and language editing. The authors are responsible for the data, source verification, interpretations and final text.

Conflicts of Interest: The authors declare no conflicts of interest.

References

1. Ismail, A.; Azadbakht, S. Experimental and Numerical Methods for Hydraulic Fracturing at Laboratory Scale: A Review. *Geosciences* **2025**, *15*, 142. [CrossRef]
2. Sun, X.; Tao, L.; Bao, J.; Qu, J.; Yang, H.; Yao, S. Evaluation of Proppant Placement Efficiency in Linearly Tapering Fractures. *Geosciences* **2025**, *15*, 275. [CrossRef]
3. Bobrova, M.; Stanchits, S.; Shevtsova, A.; Filev, E.; Stukachev, V.; Shayahmetov, T. Laboratory Investigation of Hydraulic Fracture Behavior of Unconventional Reservoir Rocks. *Geosciences* **2021**, *11*, 292. [CrossRef]
4. *GOST R 51761-2013*; Aluminosilicate Proppants. Specifications. Standartinform: Moscow, Russia, 2014.
5. *ISO 13503-5:2006*; Petroleum and Natural Gas Industries—Completion Fluids and Materials—Part 5: Procedures for Measuring the Long-Term Conductivity of Proppants. International Organization for Standardization: Geneva, Switzerland, 2006.
6. Perkins, T.K.; Kern, L.R. Widths of Hydraulic Fractures. *J. Pet. Technol.* **1961**, *13*, 937–949. [CrossRef]
7. Nordgren, R.P. Propagation of a Vertical Hydraulic Fracture. *SPE J.* **1972**, *12*, 306–314. [CrossRef]
8. Geertsma, J.; de Klerk, F. A Rapid Method of Predicting Width and Extent of Hydraulically Induced Fractures. *J. Pet. Technol.* **1969**, *21*, 1571–1581. [CrossRef]
9. Zheng, W.; Silva, S.C.; Tannant, D.D. Crushing Characteristics of Four Different Proppants and Implications for Fracture Conductivity. *J. Nat. Gas Sci. Eng.* **2018**, *53*, 125–138. [CrossRef]
10. Bandara, K.M.A.S.; Ranjith, P.G.; Rathnaweera, T.D. Laboratory-Scale Study on Proppant Behaviour in Unconventional Oil and Gas Reservoir Formations. *J. Nat. Gas Sci. Eng.* **2020**, *78*, 103329. [CrossRef]
11. Bandara, K.M.A.S.; Ranjith, P.G.; Rathnaweera, T.D.; Wanniarachchi, W.A.M.; Yang, S.Q. Crushing and Embedment of Proppant Packs under Cyclic Loading: An Insight to Enhanced Unconventional Oil/Gas Recovery. *Geosci. Front.* **2021**, *12*, 100970. [CrossRef]
12. Walsh, S.D.C.; Smith, M.; Carroll, S.A.; Crandall, D. Non-Invasive Measurement of Proppant Pack Deformation. *Int. J. Rock Mech. Min. Sci.* **2016**, *87*, 39–47. [CrossRef]
13. Voltolini, M.; Ajo-Franklin, J. Evolution of Propped Fractures in Shales: The Microscale Controlling Factors as Revealed by in Situ X-Ray Microtomography. *J. Pet. Sci. Eng.* **2020**, *188*, 106861. [CrossRef]
14. Zhang, J.; Ouyang, L.; Zhu, D.; Hill, A.D. Experimental and Numerical Studies of Reduced Fracture Conductivity Due to Proppant Embedment in the Shale Reservoir. *J. Pet. Sci. Eng.* **2015**, *130*, 37–45. [CrossRef]
15. Bui, B.T.; Tutuncu, A.N. Modeling the Swelling of Shale Matrix in Unconventional Reservoirs. *J. Pet. Sci. Eng.* **2018**, *165*, 596–615. [CrossRef]
16. Pearson, C.M.; Green, C.A.; McGill, M.; Milton-Tayler, D. Extended-Time Conductivity Testing of Proppants Used for Multi-Stage Horizontal Completions. In Proceedings of the SPE International Hydraulic Fracturing Technology Conference and Exhibition, Muscat, Oman, 11–13 January 2022; SPE-205272-MS. [CrossRef]

17. Pearson, C.M.; Green, C.A.; Milton-Tayler, D.; Trevino, V. Extended-Time Conductivity Testing of Proppants at 0.5 lb/ft^2 Used for Slickwater Multi-Stage Horizontal Completions. In Proceedings of the SPE Hydraulic Fracturing Technology Conference and Exhibition, The Woodlands, TX, USA, 31 January–2 February 2023; SPE-212334-MS. [CrossRef]
18. Pearson, C.M.; Fowler, G. The Impact of Extended-Time Proppant Conductivity Impairment on the Ultimate Recovery from Unconventional Horizontal Well Completions. In Proceedings of the SPE International Hydraulic Fracturing Technology Conference and Exhibition, Muscat, Oman, 11–13 January 2022; SPE-205294-MS. [CrossRef]
19. Kim, J.; Seo, Y.; Wang, J.; Lee, Y. History Matching and Forecast of Shale Gas Production Considering Hydraulic Fracture Closure. *Energies* **2019**, *12*, 1634. [CrossRef]
20. *GOST R 54571-2023*; Magnesial-Quarts Proppants. Specifications. Russian Institute for Standardization: Moscow, Russia, 2023. Available online: https://protect.gost.ru/gost/details/ff329485-5d96-4406-b277-63a79f9019c6 (accessed on 26 October 2026).
21. Wang, J.; Xiong, Y.; Jiao, G.; Lei, D. Assessment of Long-Term Proppant Conductivity. *Front. Energy Res.* **2022**, *10*, 813571. [CrossRef]
22. Liu, J.; Zhou, F.; Lu, X.; Zhou, X.; He, X.; Du, Y.; Xia, F.; Zhang, J.; Luo, W. Impact of Proppant Embedding on Long-Term Fracture Conductivity and Shale Gas Production Decline. *Fluid Dyn. Mater. Process.* **2025**, *21*, 2613–2628. [CrossRef]
23. Yan, C.; Zhang, P.; Dong, L.; Zhang, C.; Cheng, Y. Long-Term Fracture Conductivity in Tight Reservoirs. *Energy Sci. Eng.* **2024**, *12*, 1187–1199. [CrossRef]
24. Anaya, R.; Hernandez, M.F.; Mocciaro, A.; Richard, D.; Rendtorff, N.M. Reused Green Glass for the Production of Low-Density Ceramic Proppants. *Open Ceram.* **2024**, *19*, 100659. [CrossRef]
25. Xu, F.; Yao, K.; Li, D.; Xu, D.; Yang, H. Study on the Effect of Acid Corrosion on Proppant Properties. *Energies* **2022**, *15*, 8368. [CrossRef]
26. Ren, H.; Dong, J.; Zhang, J.; Xu, F.; Wang, B.; Liang, T. Composite Proppants Sintered from Fly Ash and Their Application in Fracturing Tight Oil Reservoirs. In Proceedings of the 58th US Rock Mechanics/Geomechanics Symposium, Golden, CO, USA, 23–26 June 2024; ARMA 24-362. [CrossRef]
27. Wang, W.; Zhou, D.; Gu, T.; Yan, Y.; Yang, X.; Xu, S. Experimental Investigation on the Influence of Proppant Crushing on the Propped Fracture Conductivity. *Processes* **2025**, *13*, 2166. [CrossRef]
28. Wei, J.-G.; Wang, X.-J.; Fu, X.-F.; Gong, P.-Q.; Zhou, X.-F.; Li, Y.-W.; Yang, Y.; Chen, Y.-H.; Jia, B.; Wu, J. Optimization of Long-Term Fracture Conductivity with Quartz: An Experimental Investigation. *Front. Energy Res.* **2022**, *10*, 973349. [CrossRef]
29. Sun, H.; He, B.; Xu, H.; Zhou, F.; Zhang, M.; Li, H.; Yin, G.; Chen, S.; Xu, X.; Li, B. Experimental Investigation on the Fracture Conductivity Behavior of Quartz Sand and Ceramic Mixed Proppants. *ACS Omega* **2022**, *7*, 10243–10254. [CrossRef] [PubMed]
30. Zhang, D.; Ma, S.; Zhang, J.; Zhu, Y.; Wang, B.; Zhu, J.; Fan, X.; Yang, H.; Liang, T. Field Experiments of Different Fracturing Designs in Tight Conglomerate Oil Reservoirs. *Sci. Rep.* **2022**, *12*, 3220. [CrossRef] [PubMed]
31. Wu, B.; Xiao, F.; Kong, M.; Wang, B.; Zhang, S. Research on Proppant Optimization and Field Test of Ultra-Deep Tight Conglomerate Sandstone Reservoir. *Front. Energy Res.* **2022**, *10*, 891063. [CrossRef]
32. Mittal, A.; Rai, C.S.; Sondergeld, C.H. Proppant-Conductivity Testing Under Simulated Reservoir Conditions: Impact of Crushing, Embedment, and Diagenesis on Long-Term Production in Shales. *SPE J.* **2018**, *23*, 1304–1315. [CrossRef]
33. Xu, J.; Ding, Y.; Yang, L.; Liu, Z.; Gao, R.; Yang, H.; Wang, Z. Conductivity Analysis of Hydraulic Fractures Filled with Nonspherical Proppants in Tight Oil Reservoir. *Energy Sci. Eng.* **2020**, *8*, 166–180. [CrossRef]
34. Bolintineanu, D.S.; Rao, R.R.; Lechman, J.B.; Romero, J.A.; Jove-Colon, C.F.; Quintana, E.C.; Bauer, S.J.; Ingraham, M.D. Simulations of the Effects of Proppant Placement on the Conductivity and Mechanical Stability of Hydraulic Fractures. *Int. J. Rock Mech. Min. Sci.* **2017**, *100*, 188–198. [CrossRef]
35. Sang, Y.; Guo, Y.; Huang, H.; Xia, D.; Chen, L.; Zhang, Z.; Gui, J. Experimental Study on the Long-Term Conductivity of Self-Support Fracture in Deep Shale Reservoirs. *J. Pet. Explor. Prod. Technol.* **2025**, *15*, 102. [CrossRef]
36. Cheng, C.; Milsch, H. Permeability Variations in Illite-Bearing Sandstone: Effects of Temperature and NaCl Fluid Salinity. *J. Geophys. Res. Solid Earth* **2020**, *125*, e2020JB020122. [CrossRef]
37. Cheng, C.; Milsch, H. Evolution of Fracture Aperture in Quartz Sandstone under Hydrothermal Conditions: Mechanical and Chemical Effects. *Minerals* **2020**, *10*, 657. [CrossRef]

Disclaimer/Publisher's Note: The statements, opinions and data contained in all publications are solely those of the individual author(s) and contributor(s) and not of MDPI and/or the editor(s). MDPI and/or the editor(s) disclaim responsibility for any injury to people or property resulting from any ideas, methods, instructions or products referred to in the content.